Convolutional versus Self-Organized Operational Neural Networks for Real-World Blind Image Denoising

Junaid Malik, Serkan Kiranyaz, *Senior Member, IEEE*, Mehmet Yamac, Esin Guldogan, Moncef Gabbouj, *Fellow, IEEE*

Abstract— Real-world blind denoising poses a unique image restoration challenge due to the non-deterministic nature of the underlying noise distribution. Prevalent discriminative networks trained on synthetic noise models have been shown to generalize poorly to real-world noisy images. While curating real-world noisy images and improving ground truth estimation procedures remain key points of interest, a potential research direction is to explore extensions to the widely used convolutional neuron model to enable better generalization with fewer data and lower network complexity, as opposed to simply using deeper Convolutional Neural Networks (CNNs). Operational Neural Networks (ONNs) and their recent variant, Self-organized ONNs (Self-ONNs), propose to embed enhanced non-linearity into the neuron model and have been shown to outperform CNNs across a variety of regression tasks. However, all such comparisons have been made for compact networks and the efficacy of deploying operational layers as a drop-in replacement for convolutional layers in contemporary deep architectures remains to be seen. In this work, we tackle the real-world blind image denoising problem by employing, for the first time, a deep Self-ONN. Extensive quantitative and qualitative evaluations spanning multiple metrics and four highresolution real-world noisy image datasets against the state-ofthe-art deep CNN network, DnCNN, reveal that deep Self-ONNs consistently achieve superior results with performance gains of up to 1.76dB in PSNR. Furthermore, Self-ONNs with half and even quarter the number of layers that require only a fraction of computational resources as that of DnCNN can still achieve similar or better results compared to the state-of-the-art.

Index Terms—Image enhancement, Operational neural networks, Real-world image denoising.

I. INTRODUCTION

Image denoising is one of the key low-level image restoration tasks because noise is inherent to every image acquisition system. A foremost challenge in designing denoising methods is the fact that obtaining a true noise-free image is an ill-posed problem because the noise in real-world images

to the original image to produce its noisy counterpart [1]-[4]. While this approach has been a standard for decades, it makes strong assumptions that are inconsistent with empirical observations about real-world noisy images [5]-[7]. Most importantly, noise in real-world images does not necessarily follow the normal distribution, is data dependent and not stationary. Moreover, the additive approach for synthesizing noisy images assumes the original image to be free of any kind of noise, which is rarely the case. Because of this, discriminative learning-based denoising methods that are trained on synthetic noisy images fail to maintain their performance levels when tested on real-world images [5], [8]. To remedy this, several image datasets have been proposed in recent years, which employ different ground truth estimation procedures to produce clean images from realworld noisy images [5], [9], [10]. Discriminative methods trained on these new datasets have exhibited a better generalization performance than those trained using synthetic additive noise data [5]. While the efforts for producing better estimations for ground-truth images continue, it is worth noting that the key ingredients behind the denoising methods have not yet progressed. Almost all discriminative learning-based methods utilize

is non-deterministic. One of the most widely accepted ways

to deal with this is through the use of synthetic noise models,

where a known noise distribution (generally WGN), is added

Almost all discriminative learning-based methods utilize Convolutional Neural Networks (CNNs), which have become a *de-facto* standard for many computer vision tasks. However, recent studies have identified drawbacks in the convolutional neuron model [11], especially for denoising [12]. Being a variant of the multi-layer perceptron (MLP) with two known restrictions (i.e., limited connection and weight sharing), convolutional neurons essentially apply a linear transformation to the input (i.e., the output map of the previous layer neuron), whereas the point-wise activation function or non-linear pooling operations following the

Serkan Kiranyaz (mkiranyaz@qu.edu.qa) is with the Department of Electrical Engineering, Qatar University, Doha, Qatar.

Mehmet Yamac (mehmet.yamac@huawei.com) and Esin Guldogan (esin.guldogan@huawei.com) are with HUAWEI Technologies, Tampere, Finland.

The paper was submitted on 04.03.2021 for review.

Junaid Malik (junaid.malik@tuni.fi) and Moncef Gabbouj (moncef.gabbouj@tuni.fi) are with the Department of Computing Sciences, Tampere University, Tampere, Finland.

convolution are the unique source of non-linearity in the network. This is often cited as one of the major reasons why state-of-the-art CNNs need to be deep, over-parameterized, and hence require a large amount of training data to achieve a decent generalization. Many possible solutions have been explored recently [13], [14] to increase non-linearity in CNNs without adding more layers. One of the key developments in this regard is the conception of so-called Operational Neural Networks (ONNs) [11]. ONNs are composed of generalized (operational) neurons that allow the flexibility to incorporate any non-linear patch-wise transformation. When properly configured with optimal non-linear functions, ONNs were shown to outperform equivalent CNNs across a variety of challenging tasks and under severe training constraints. More importantly, unlike [13], [14], ONNs allow a heterogeneous network model where each neuron applies a unique transformation to the input, resulting in enhanced diversity of intra-layer activations. An important factor that determines the performance of ONN is the choice of non-linear operators. There have been numerous search methodologies explored, including GIS [11] and synaptic plasticity monitoring (SPM) [15] to identify the best operators for a given learning problem. However, they require additional training runs to ensure convergence towards suitable operators. To address this drawback, a self-organized variant of ONNs, the Self-ONN, has been proposed recently [12], [16]. Self-ONNs employ the Taylor series function approximation to generate non-linear transformations during the training. Self-ONNs were successfully applied for a variety of severe image restoration problems in [12]. Compact (two-layer) Self-ONNs outperformed CNNs across diverse noise models with a significant gap. The work established, based on various ablation tests, that with limited training data and compact networks, Self-ONNs can learn and generalize better than CNNs. However, the value of the proposed Self-ONNs for deeper network architectures and more realistic noise characteristics remains to be seen.

In this study, we investigate the efficacy of Self-ONNs for denoising real-world noisy images, as compared to CNNs. To this end, we consider the current state-of-the-art 17-layer deep denoising architecture introduced in [4] and convert it to a Self-ONN by replacing convolutional layers with the (self-organized) operational layers. All networks are subsequently trained with the same training data and equivalent training conditions to highlight the true impact of introducing the operational layers. The primary contributions of this work are enumerated as follows:

- We configure and train a novel deep Self-ONN for real-world image denoising. This is the first study that proposes a deep ONN for any regression task. This is also the first study that proposes an ONN for real-world denoising problems.
- We evaluate and compare Self-ONN with DnCNN across 4 high-resolution real-world denoising benchmark data and find that a Self-ONN, even with

- less number of layers, surpasses DnCNN, especially in terms of perceptual quality metrics.
- We analyze and discuss the effect of enhanced nonlinearity and heterogeneity in deep Self-ONNs quantitatively by calculating the strengths of the synaptic connections.
- We provide an alternative vectorized formulation of Self-ONNs which lends itself to efficient parallelization on dedicated hardware resources such as GPUs.

The remaining of the paper is organized as follows: Section II briefly presents the related work including the benchmark datasets in real-world image denoising. Section III introduces the Self-ONNs and generative neurons in detail and formulates the vectorized notation. Section IV introduces the experimental setup and the DnCNN network architecture. Section V presents detailed comparative evaluations among Self-ONNs against DnCNN over four benchmark datasets and discusses the results. Moreover, the computational complexity analysis of the networks is also presented in this section. Finally, Section VI concludes the paper and suggests topics for future research.

II. RELATED WORK

A. Datasets

The RENOIR dataset [10] consists of images from two digital cameras and one smartphone. It contains 120 images corresponding to as many scenes. Noisy images were acquired by using a short-time exposure camera setting to capture low-light scenes. The corresponding reference images are acquired by long-time exposure to the same scene. Intensity alignment is applied as a post-processing step to produce "ground-truth" images. The CCNoise dataset [17] contains images from 11 natural scenes captured through 3 cameras. It consists of 17 images acquired by taking 500 consecutive images taken from the same scene. Assuming that the noise is zero-mean, ground truth estimation is done by taking the temporal mean of these 500 images. The DND dataset [5] consists of images from 50 unique scenes. Reference/clean image is acquired by capturing the scene using a base ISO level. The corresponding noisy image is taken using a higher ISO/lower exposure time. For ground truth estimation, a thorough post-processing procedure consisting of removal of low-frequency residual noise and intensity alignment is used. For benchmarking, 512x512 test crops are provided whereas the ground truth images are not made public and are held out for benchmarking through online submission. SIDD dataset [9] was curated exclusively for smartphone images by capturing 10 different scenes with 15 different ISO values (corresponding to different levels of noise). Images were acquired using five different smartphones with different illumination temperatures and brightness levels, leading to a vast variety of noisy images. In addition, an extensive ground-truth estimation procedure was

adopted to obtain clean images. The "MEDIUM" variant of the dataset consists of 320 high-resolution noisy-clean image pairs.

B. Real-World Denoising Methods

Numerous denoising techniques were benchmarked on the RENOIR dataset in [10]. The pioneering non-local technique, BM3D [18], achieved considerably superior results compared to all other techniques, providing an appropriate estimate of the noise level. In particular, the discriminative method of MLP [3], which was proven to be competitive with BM3D on synthetic noise, could not retain the performance on realworld noisy images. Its performance fell on average by 2.06dB in terms of PSNR and around 5% in terms of the perceptual quality index (SSIM). Benchmarking on later datasets [5], [9] confirmed these findings, despite employing vastly different ground-truth estimation methods. Even complex deep CNN-based methods such as DnCNN [4] trained on synthetic AWGN noise models did not provide adequate denoising performance. Nevertheless, the same architecture performed considerably better when trained on real-world instead of synthetic noisy-clean image pairs. Considering these findings, contemporary methods generally aim at utilizing available real-world noisy images [19]–[23], devising realistic noise models to synthesize artificial noisy images [8], [21], [24], [25], and designing appropriate architectural changes [8], [19]-[23], [25]. It is worth noting that the common denominator among all these networks is the sole usage of the convolutional layer as the core transformation. Their novelty is limited to architectural upgrades such as residual connections [23], feature attention [20], multi-scale approach [25], or some combination of these techniques. In contrast, in this study, while keeping the network architecture of DnCNN intact, we propose a fundamental paradigm shift by proposing the operational layers of Self-ONNs instead of the convolutional layers to enhance the expressivity of the denoising models. To validate our claim, we employ the deep CNN architecture of DnCNN [4] and convert it to a Self-ONN with the drop-in replacement of all convolutional layers. To expel the subjectivity arising from the choice of training data and hyperparameters, all the networks in this study are identically trained from scratch using the same training resources. We show that Self-ONNs surpass both DnCNN and their CNN counterparts, and remain competitive even when trimmed down to four-times fewer layers, especially in terms of perceptual quality of the denoised images.

III. SELF-ORGANIZED OPERATIONAL NEURAL NETWORKS

In this section, we will proceed by revisiting how ONNs generalize the convolution operation. Afterward, the mathematical model of the generative neuron-based Self-ONN will be presented.

We consider the case of the k^{th} neuron in the l^{th} layer of a 2D convolutional neural network. To be concise, we assume

the 'same' convolution operation with unit stride and the required amount of zero padding. The output of this neuron can be formalized as follows:

$$x_k^l = b_k^l + \sum_{i=0}^{N_{l-1}} x_{ik}^l \tag{1}$$

where b_k^l is the bias associated with this neuron and x_{ik}^l is defined as:

$$x_{ik}^{l} = Conv2D(w_{ik}, y_i^{l-1})$$
 (2)

Here, $w_{ik} \in \mathbb{R}^{K \times K}$ is the kernel connecting the i^{th} neuron of $(l-1)^{th}$ layer to k^{th} neuron of l^{th} layer, while $x_{ik}^{l} \in \mathbb{R}^{M \times N}$ is the input map, and $y_{i}^{l-1} \in \mathbb{R}^{M \times N}$ are the l^{th} and $(l-1)^{th}$ layers' k^{th} and i^{th} neurons' outputs respectively. By definition, the convolution operation of (2) can be expressed as follows:

$$x_{ik}^{l}(m,n) = \sum_{r=0}^{K-1} \sum_{t=0}^{K-1} w_{ik}^{l}(r,t) y_{i}^{l-1}(m+r,n+t)$$
 (3)

The main idea behind an operational neuron is a generalization of the above as follows:

$$\overline{x_{ik}^l}(m,n) = P_k^l \left(\psi_k^l \left(w_{ik}^l(r,t), y_i^{l-1}(m+r,n+t) \right) \right)_{(r,t)=(0,0)}^{(K-1,K-1)}$$
(4)

where $\psi_l^k(\cdot) : \mathbb{R}^{MN \times K^2} \to \mathbb{R}^{MN \times K^2}$ and $P_k^l(\cdot) : \mathbb{R}^{MN \times K^2} \to$ \mathbb{R}^{MN} are termed as *nodal* and *pool* functions, respectively, assigned to the k^{th} neuron of l^{th} layer. In a heterogenous ONN configuration, every neuron has uniquely assigned ψ and P operators. Owing to this, an ONN network enjoys the flexibility of incorporating any non-linear transformation, which is suitable for the given learning problem at hand. However, hand-crafting a suitable library of possible operators and searching for an optimal one for each neuron in a network introduces a significant overhead, which rises with increasing network complexity. exponentially Moreover, it is also possible that the right operator for the given learning problem cannot be expressed in terms of wellknown functions. To resolve this key limitation, a composite nodal function is required that is iteratively created and tuned during back-propagation. A straightforward choice for accomplishing this would be to use a weighted combination of all operators in the operator set library and learning the weights during training. However, such a formulation would be susceptible to instability issues because of different dynamic ranges of individual functions. Additionally, it would still rely on the manual selection of suitable functions to populate the library. Therefore, to formulate a nodal transformation that does not require a pre-selection and manual assignment of operators, we make use of the Taylorseries-based function approximation. The Taylor series expansion of an infinitely differentiable function f(x) about a point a is given as:

$$f(x) = \sum_{n=0}^{\infty} \frac{f^{(n)}(a)}{n!} (x - a)^n$$
 (5)

The Q^{th} order truncated approximation of (5), formally known as the Taylor polynomial, takes the following form:

$$f(x)^{(Q,a)} = \sum_{n=0}^{Q} \frac{f^{(n)}(a)}{n!} x^n$$
 (6)

The above formulation enables the approximation of any function f(x) sufficiently well in the close vicinity of a. If the coefficients $\frac{f^{(n)}}{n!}$ are tuned and the inputs are bounded, the formulation of (6) can be used to *generate* any transformation. This is the key idea behind the generative neurons which form Self-ONNs. Specifically, in terms of notation used in (4), the nodal transformation of a generative neuron would take the following general form:

$$\widetilde{\psi}_{k}^{l}\left(w_{ik}^{l(Q)}(r,t), y_{i}^{l-1}(m+r,n+t)\right) = \sum_{q=1}^{Q} w_{ik}^{l(Q)}(r,t,q) \left(y_{i}^{l-1}(m+r,n+t)\right)^{q}$$
(7)

In (7), Q is a hyperparameter which controls the degree of the Taylor approximation, and $w_{ik}^{l(Q)}$ is a learnable kernel of the network. A key difference in (7) as compared to the convolutional (3) and operational (4) model is that $\widetilde{\psi_k^l}$ is not fixed, rather a distinct operator over each individual output, y_i^{l-1} , and thus requires Q times more parameters. Therefore, the $K \times 1$ kernel vector w_{ik}^l has been replaced by a $K \times Q$ matrix $w_{ik}^{l(Q)} \in \mathbb{R}^{K \times Q}$ which is formed by replacing each element $w_{ik}^l(r)$ with a Q-dimensional vector $w_{ik}^{l(Q)}(r) = [w_{ik}^{l(Q)}(r,0), w_{ik}^{l(Q)}(r,1), \dots, w_{ik}^{l(Q)}(Q-1)]$. The input map of the generative neuron, \widetilde{x}_{ik}^l can now be expressed as,

$$\widetilde{x_{lk}^l}(m,n) =$$

$$P_k^l \left(\sum_{q=1}^Q w_{ik}^{l(Q)}(r,t,q) \left(y_i^{l-1}(m+r,n+t) \right)^q \right)^{(K-1,K-1)}$$
(8)

During training, as $w_{ik}^{l(Q)}$ is iteratively tuned by backpropagation (BP), customized nodal transformation functions will be generated as a result of (8), which would be tailored for $i-k^{th}$ connection. This enables enhanced flexibility which provides three key benefits. First, the need for manually defining a list of suitable nodal operators and searching for the optimal operator for each neuronal connection is naturally alleviated. Secondly, heterogeneity is not limited to each neuronal connection i – down to each kernel element $\tilde{\psi}_l^k \left(w_{ik}^{l(Q)}(r,t), y_i^{l-1}(m+r,n+t) \right)$ will unique be

 $\forall (r,t) \in [(0,0),...,(0,K-1),...,(K-1,0),...,(K-1,K-1)]$. Such diversity is not achievable even with the flexible operational neuron model of ONNs. Thirdly, in generative neurons, the heterogeneity is driven only by the values of the weights $w_{ik}^{l(Q)}$ and the core operations (multiplication, summation) are the same for all neurons in a layer, as shown in (8). Owing to this, unlike ONNs, the generative neurons inside a Self-ONN layer can be parallelized more efficiently, leading to a considerable reduction in computational complexity and time. Moreover, a specific case of formulation (8) can also be expressed in terms of the widely applicable convolutional model.

A. Representation of Self-ONN Using Convolutions

Consider the pooling operator P_k^l to be the summation operator. \tilde{x}_{ik}^l is then defined as:

$$\widetilde{x_{lk}^{l}}(m) = \sum_{r=0}^{K-1} \sum_{t=0}^{K-1} \sum_{q=1}^{Q} w_{lk}^{l(Q)}(r,t,q) \left(y_i^{l-1}(m+r,n+t) \right)^{q}$$

$$(9)$$

Exploiting the commutativity of the summation operations in (9), we can alternatively write:

$$\widetilde{x_{lk}^l}(m) = \sum_{q=1}^{Q} \sum_{r=0}^{K-1} \sum_{t=0}^{K-1} w_{lk}^{l(Q)}(r, t, q-1) y_l^{l-1}(m+r, n+t)^q \quad (10)$$

Using (1) and (2), the formula in (10) can be further simplified as follows:

$$\widetilde{\chi_{lk}^l} = \sum_{q=1}^{Q} Conv2D(w_{lk}^{l(Q)}, (y_i^{l-1})^q)$$
 (11)

Hence, the formulation can be accomplished by applying Q 2D convolution operations. If Q is set to 1, (11) entails the convolutional formulation of (3). Therefore, as CNN is a subset of ONN corresponding to a specific operator set, it is also a special case of a Self-ONN with Q=1 set for all neurons.

B. Vectorized Notation

Expressing explicit loops in terms of matrix and vector manipulations is a key idea behind vectorization, which is a major driving factor behind the fast implementations of modern-day neural network implementations. In this section, we first introduce how the vectorized notation can be used to express the 2D convolution operation inside a neuron. Afterward, the same key principles will be exploited to express the generative neuron formulation of (9) as a single matrix-vector product. First, an alternate formulation of the operation of (3) is now presented. We introduce a

transformation $\delta(\cdot, K^2)$ using which y_i^{l-1} is reshuffled such that values inside each $K \times K$ - kernel across y_i^{l-1} are vectorized and concatenated as rows to form a matrix $Y_i^{l-1} \in \mathbb{R}^{M \times N \times K}$. The process is visually depicted in Fig. 7 for K = 2, and mathematically expressed in (12).

 $Y_i^{l-1} = \delta(v_i^{l-1}, K^2)$

Secondly, we construct a matrix $W_{ik}^l \in \mathbb{R}^{M \times K}$ whose rows are repeated copies of the vectorized version of $w_{ik} \in \mathbb{R}^{K \times K}$.

$$W_{ik}^{l} = \begin{bmatrix} w_{ik}^{l}(0,0) & w_{ik}^{l}(0,K-1) & \cdots & w_{ik}^{l}(K-1,K-1) \\ \vdots & \vdots & \cdots & \vdots \\ w_{ik}^{l}(0,0) & w_{ik}^{l}(1,K-1) & \cdots & w_{ik}^{l}(K-1,K-1) \\ \vdots & \vdots & \cdots & \vdots \\ w_{ik}^{l}(0,0) & w_{ik}^{l}(1,K-1) & \cdots & w_{ik}^{l}(K-1,K-1) \end{bmatrix}$$
(13)

We now consider the Hadamard product of these two matrices:

$$Y_i^{l-1} \otimes W_{ik}^l$$

$$= \begin{bmatrix} y_i^{l-1}(0,0)w_{ik}^l(0,0) & \cdots & y_i^{l-1}(K-1,K-1)w_{ik}^l(0,0) & \cdots & y_i^{l-1}(K-1,K-1)w_{ik}^l(0,0) & \cdots & y_i^{l-1}(M+K-1,N+K-1) \\ \vdots & \cdots & \vdots & \cdots & \vdots \\ y_i^{l-1}(M-1,N-1)w_{ik}^l(0,0) & \cdots & y_i^{l-1}(M+K-1,N+K-1) \end{bmatrix}$$
(14)

Applying summation operation across rows, we get:

$$\sum_{r=0}^{K-1} \left(Y_i^{l-1} \otimes W_{ik}^l \right)$$

$$= \begin{bmatrix} \sum_{r=0}^{K-1} \sum_{t=0}^{K-1} y_i^{l-1}(r,t) w_{ik}^l(r,t) \\ \vdots \\ \sum_{r=0}^{K-1} \sum_{t=0}^{K-1} y_i^{l-1}(m+r,n+t) w_{ik}^l(r,t) \\ \vdots \\ \sum_{r=0}^{K-1} \sum_{t=0}^{K-1} y_i^{l-1}(M+r,N+t) w_{ik}^l(r,t) \end{bmatrix}$$

$$= \sum_{r=0}^{K-1} w_{ik}^l(r) y_i^{l-1}(m+r)$$
(15)

Reshaping this back to $\mathbb{R}^{M\times N}$, we get

$$vec_{M\times N}^{-1}\left(\sum_{k=1}^{K-1}\left(Y_{i}^{l-1}\otimes W_{ik}^{l}\right)\right)(m,n)$$

$$=\sum_{k=0}^{K-1}\sum_{l=0}^{K-1}y_{i}^{l-1}(m+r,n+t)w_{ik}^{l}(r,t)$$
(16)

which is equivalent to (3). We also note that,

$$\sum Y_i^{l-1} \otimes W_{ik}^l = Y_i^{l-1} \overline{W_{ik}^l} \tag{17}$$

Therefore.

$$x_{ik}^l(m,n) = vec_{M \times N}^{-1} \left(Y_i^{l-1} \overrightarrow{w_{lk}^l} \right) (m,n)$$
 (18)

$$x_{ik}^{l} = vec_{M \times N}^{-1} \left(Y_i^{l-1} \overrightarrow{W_{ik}} \right)$$
 (19)

We show here a representation of 2D convolution operation through a neuron by a single matrix-vector product. This operation lies at the heart of conventional generalized matrix multiplication (GEMM)-based convolution implementations and enables efficient usage of parallel computational resources such as GPU cores.

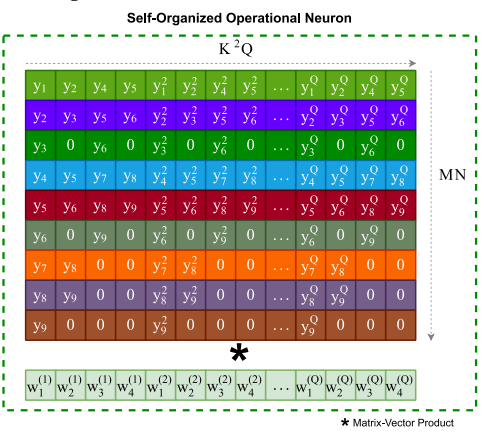


Figure 1. A visual illustration of the transformations required for convolutional and self-organized operational neurons. Both neuron models require a single matrix-vector product.

C. Forward Propagation through a 2D Self-ONN neuron We showed in (11) how the Self-ONN formulation of (10) can be represented as a summation of Q individual convolutional operations. Moreover, from (12), a convolutional operation can be represented as a matrix-vector product. We now use these two formulations to represent the transformation of (11) as a single convolution operation, and consequently a single matrix-vector product, instead of Q-separate ones. We start by introducing $Y_i^{l-1(Q)} \in \mathbb{R}^{MN \times K^2 Q}$ such that

$$Y_i^{l-1(Q)} = [Y_i^{l-1} \quad (Y_i^{l-1})^{\circ 2} \quad \dots \quad (Y_i^{l-1})^{\circ Q}]$$
 (20)

where $\circ n$ is the Hadamard exponentiation operator. The m^{th} row of Y_i^{l-1} can be expressed as

This is also illustrated in Figure 1. Moreover, we construct $\frac{W_{ik}^{l(Q)}}{w_{ik}^{l(Q)}} \in \mathbb{R}^{MN \times KQ}$ by first vectorizing $w_{ik}^{l(Q)} \in \mathbb{R}^{K \times K \times Q}$ to $\overline{w_{ik}^{l(Q)}} \in \mathbb{R}^{K^2Q}$ and then concatenating m copies of $\overline{w_{ik}^{l(Q)}}$ along the row dimension, as expressed in (22) and (23).

$$\overline{w_{ik}^{l(Q)}} = \begin{bmatrix}
w_{ik}^{l(Q)}(0,0,0) \\
\vdots \\
w_{ik}^{l(Q)}(K-1,K-1,0) \\
w_{ik}^{l(Q)}(0,0,1) \\
\vdots \\
w_{ik}^{l(Q)}(K-1,K-1,1) \\
\vdots \\
w_{ik}^{l(Q)}(0,0,Q-1) \\
\vdots \\
w_{ik}^{l(Q)}(K-1,K-1,Q-1)
\end{bmatrix} (22)$$

$$W_{ik}^{l(Q)}(m) = \overline{w_{ik}^{l(Q)}}$$

The matrix-vector product of $Y_i^{l-1^{(Q)}}$ and $\overline{w_{ik}^{l(Q)}}$, is now given as:

$$Y_{i}^{l-1(Q)}\left(\overline{w_{ik}^{l(Q)}}\right)$$

$$= \begin{bmatrix} \sum_{q=1}^{Q} \sum_{r=0}^{K-1} \sum_{t=0}^{K-1} y_{i}^{l-1}(r,t)w_{ik}^{l}(r,t,q-1) \\ \vdots \\ \sum_{q=1}^{Q} \sum_{r=0}^{K-1} \sum_{t=0}^{K-1} y_{i}^{l-1}(m+r,n+t)w_{ik}^{l}(r,t,q-1) \\ \vdots \\ \sum_{q=1}^{Q} \sum_{r=0}^{K-1} \sum_{t=0}^{K-1} y_{i}^{l-1}(M+r,N+t)w_{ik}^{l}(r,t,q-1) \end{bmatrix}$$
(24)

From (24), after reshaping back to $\mathbb{R}^{M \times N}$ we can note that:

$$\operatorname{vec}_{\mathsf{M}\times\mathsf{N}}^{-1}\left(Y_{i}^{l-1^{(Q)}}\left(\overline{w_{ik}^{l(Q)}}\right)\right)(m,n)$$

$$=\sum_{q=1}^{Q}\sum_{r=0}^{K-1}\sum_{l=0}^{K-1}y_{i}^{l-1}(m+r,n+t)w_{ik}^{l}(r,t,q-1)$$
(25)

This is equivalent to (10). So, one can now express,

$$\widetilde{\chi_{lk}^{l}} = vec_{M \times N}^{-1} \left(Y_l^{l-1(Q)} \left(\overline{W_{lk}^{l(Q)}} \right) \right)$$
 (26)

The formulation of (26) provides a key computational benefit, as the forward propagation through the generative neuron is accomplished using a single matrix-vector product. Hence, in theory, if the computational cost and memory requirement of constructing and storing matrices $Y_i^{l-1}(Q)$ and $W_{ik}^{l(Q)}$ are considered negligible, the complexity of a convolutional neuron is approximately the same as that of the generative neuron, as both can be accomplished by a single matrix-vector product that is fully parallelizable. Finally, to complete the forward propagation step, using (1), we can express:

$$\widetilde{x_k^l} = b_k^l + \sum_{i=0}^{N_{l-1}} \widetilde{x_{ik}^l}$$
 (27)

IV. EXPERIMENTS

All experiments were conducted in Python using the FastONN library [26]. Access to source codes is available at request from www.github.com/junaidmalik09/rwdenoise.

A. Network Architecture

We use DnCNN deep network [4] as the baseline CNN architecture. To keep the comparison fair between the two network models, we do not selectively convert specific convolutional layers to operational layers. Instead, we use the operational layers of Self-ONNs as a drop-in replacement for all the convolutional layers in the network. Additionally, different variants of the Self-ONN networks, Dn-SelfONN-

M, are explored, each having M operational layers. For Self-ONN networks, the value of Q is set to 3 by default. For Dn-SelfONN-4, a higher Q value of 5 is also used. Further details are presented in Table 1.

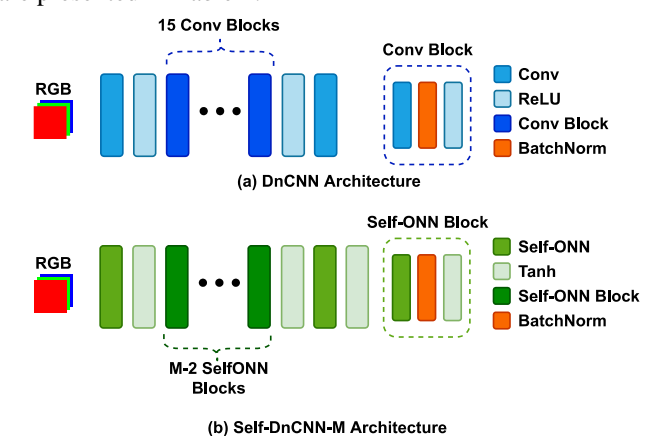


Figure 2 Network architecture for (a) the original DnCNN [4] network, and (b) the Dn-SelfONN-M network.

B. Settings

For training the network, 512 patches of size 80x80 are extracted at random from each of the 320 images of the

SIDD-Medium dataset. This effectively gives a total of 160K training patches which are randomly split with a ratio of 9:1 for training and validation respectively. All the networks are trained for 500 epochs and the model achieving the best validation PSNR is chosen.

Table 1. Details of the network architectures used in this study.

Network	Layers	Neurons	Q	Params (k)
DnCNN	17	1024	-	558
Dn-SelfONN-17	17	1024	3	1671
Dn-SelfONN-8	8	512	3	675
Dn-SelfONN-4_3	4	256	3	232
Dn-SelfONN-4_5	4	256	5	386

V. RESULTS AND DISCUSSION

We present two sets of comparisons in this section. First, a comparison of Self-ONN networks with the baseline CNN network is presented across the datasets detailed in Section A. Afterward, we evaluate the trained models on public benchmarks provided by SIDD and DnD datasets and compare Self-ONN networks with the baseline CNN as well as contemporary works.

Table 2. Comparison of baseline CNN with corresponding Self-ONN architectures.

	REI	NOIR	(CC	Sl	DD
	PSNR	SSIM	PSNR	SSIM	PSNR	SSIM
Noisy (Input)	27.38	0.7459	34.68	0.9436	23.66	0.5413
DnCNN (Baseline CNN)	32.34	0.9034	36.25	0.9689	36.06	0.9380
Dn-SelfONN-17	34.10↑	0.9317↑	37.52↑	<i>0.9800</i> ↑	36.95↑	<i>0.9506</i> ↑
Dn-SelfONN-8	33.88↑	<i>0.9350</i> ↑	35.20↓	0.9760↑	36.24↑	0.9491↑
Dn-SelfONN-4_3	33.06↑	0.9227↑	33.83↓	0.9679↓	35.39↓	0.9437↑
Dn-SelfONN-4_5	33.26↑	0.9261↑	34.85↓	0.9711↑	35.41↓	0.9444↑

C. Denoising Performance

1) DnCNN vs Dn-SelfONN-17

Experimental results for all tested models across the three datasets are shown in Table 2. One can observe that the Self-ONN model Dn-SelfONN-17 outperforms DnCNN by a substantial margin across all datasets and for both evaluation metrics. On average, improvements of 1.31 dB in terms of PSNR and 1.73% in terms of SSIM are observed across the three datasets. Hence, the deep Self-ONN network surpasses DnCNN with an equal number of layers and neurons. This establishes the superiority of the operational layers over the convolutional layers for the denoising problem.

2) DnCNN versus Dn-SelfONN-M

As explained in Section III, a Self-ONN layer (with Q>1) introduces extra trainable parameters as compared to a CNN. If the number of parameters is considered as the metric of equivalence, then the comparison presented in Section C might be deemed unfair. As an alternate ablation test, we

reduced the number of layers and neurons in Self-ONN variants as described in Table 1 to make the comparison fair in terms of the cumulative number of trainable parameters in the network. From Table 2, we can see that the Self-ONN network with 8 layers (Dn-SelfONN-8) with half the neurons still surpasses the 17-layer CNN in all but one dataset in terms of PSNR, and all datasets in terms of SSIM metric.

To take the deep CNN *versus* compact Self-ONN comparison a step further, we trimmed the Self-ONN network down to 4 layers only with a quarter of the neurons used in DnCNN. This is obviously an unfair comparison as DnCNN is not only deeper than the Self-ONN network with four-times more learning units, but also has a significantly higher number of trainable parameters. We can see from Table 2 that both of the 4-layer Self-ONN variants (Dn-SelfONN-4_3 and Dn-SelfONN-4_5) still produce competitive results. Dn-SelfONN-4_3 surpasses the deep CNN in terms of SSIM on two datasets, and in terms of PSNR on one dataset. Specifically, improvements of 2.2% PSNR

and 2.5% SSIM on the RENOIR dataset, and 0.6% SSIM on the SIDD dataset are observed, with a significant reduction of 58.5% over the trainable parameters, as compared to the baseline CNN. Increasing the value of Q to 5 improves the results further, albeit at the expense of additional trainable parameters. However, as shown in Table 1, the total number of parameters is still less than that of DnCNN so the comparison remains biased. Dn-SelfONN-4_5 outperforms the deep CNN with respect to PSNR on the RENOIR dataset and in terms of SSIM on *all* three datasets. Specifically, improvements of 2.84% PSNR and 2.5% SSIM on the

RENOIR dataset, 0.22% SSIM on the CCNoise dataset, and 0.68% SSIM on the SIDD dataset are observed, with 30.8% fewer parameters than that of the baseline CNN. It is worth noting here that Self-ONNs manage to achieve a higher SSIM value than the baseline CNN, even in the cases when PSNR is lower. This can be attributed to the fact that the Self-ONN neuron model is more capable of recovering perceptual information, such as textures and local details, from the corrupted image, instead of over-smoothing which might result in better PSNR values but lower SSIM. This will be validated with the qualitative results presented next.

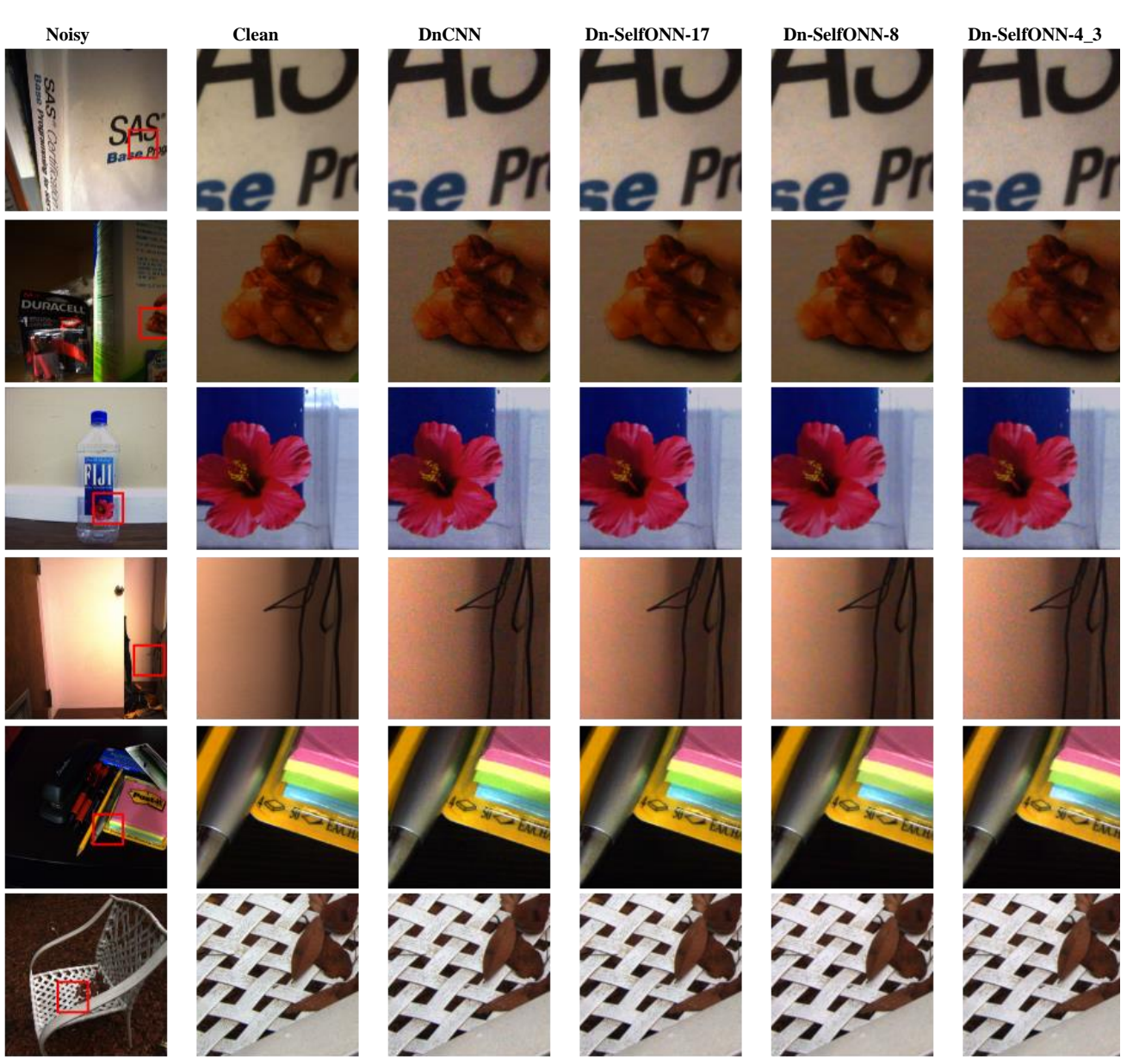


Figure 3. Visual comparison of denoising results on high-resolution noisy images from the RENOIR [10] dataset.

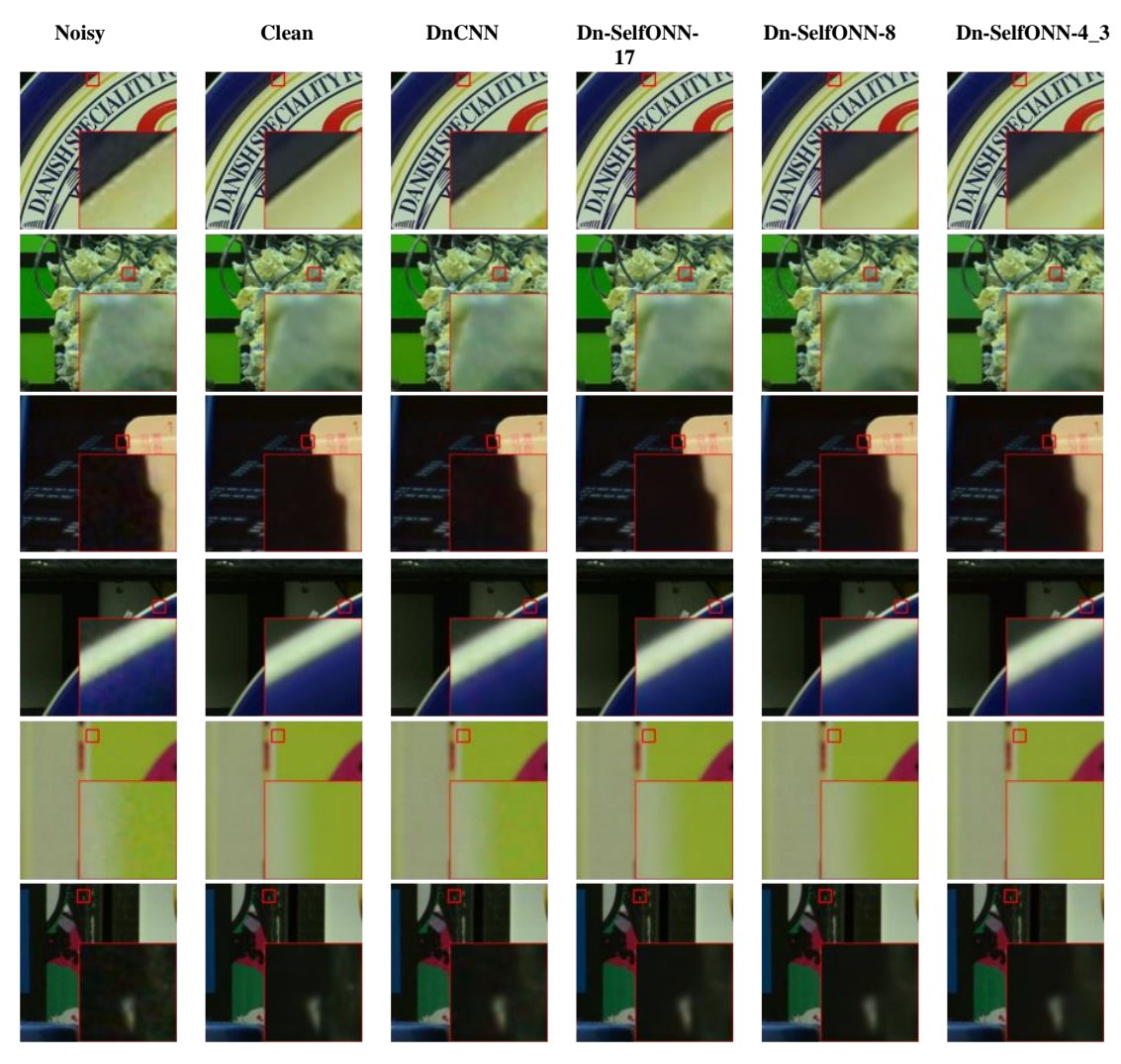


Figure 4. Denoising results of the networks used in this study on example images from the CCNoise [17] dataset.

3) Comparison on DND public benchmark

We also evaluated the performance of DnCNN along with the Self-ONN variants on the DND benchmark dataset using their online submission system. The results of the networks used in this study and some of the well-known denoising methods are presented in Table 3. Dn-SelfONN-17 surpasses the baseline CNN by a significant margin of 0.38dB while the 8-layer Self-ONN marginally surpasses the baseline CNN. Also, the best performing 4-layer network, Dn-SelfONN-4_5 results in a decrease of only 1.2% PSNR with 4 times fewer layers and a 44.5% decrease in the number of trainable parameters. Another important observation from Table 3 is that the CNN baseline used in this study, DnCNN, surpasses the method of CBDNet [21] despite the latter employing a highly enriched mixture of real and synthetic noisy images and significantly more sophisticated network architecture. Although beyond the scope of this study, this nevertheless points out a pertinent need for a fairer benchmarking of new

architectures and the importance of revisiting older ones with better training data.

Table 3. Results on DND public benchmark.

Network	PSNR	SSIM
Noisy	29.84	0.7018
BM3D [18]	34.51	0.8507
MLP [3]	34.23	0.8331
TNRD [27]	33.65	0.8306
KSVD	36.49	0.8978
FFDNet+ [28]	37.61	0.9415
DnCNN+	37.90	0.9430
TWSC [29]	37.94	0.9416
CBDNet [21]	38.06	0.9421
DnCNN (Baseline)	38.10	0.9323
Dn-SelfONN-17	38.48	0.9404
Dn-SelfONN-8	38.12	0.9356
Dn-SelfONN-4_3	37.56	0.9288
Dn-SelfONN-4_5	37.62	0.9283

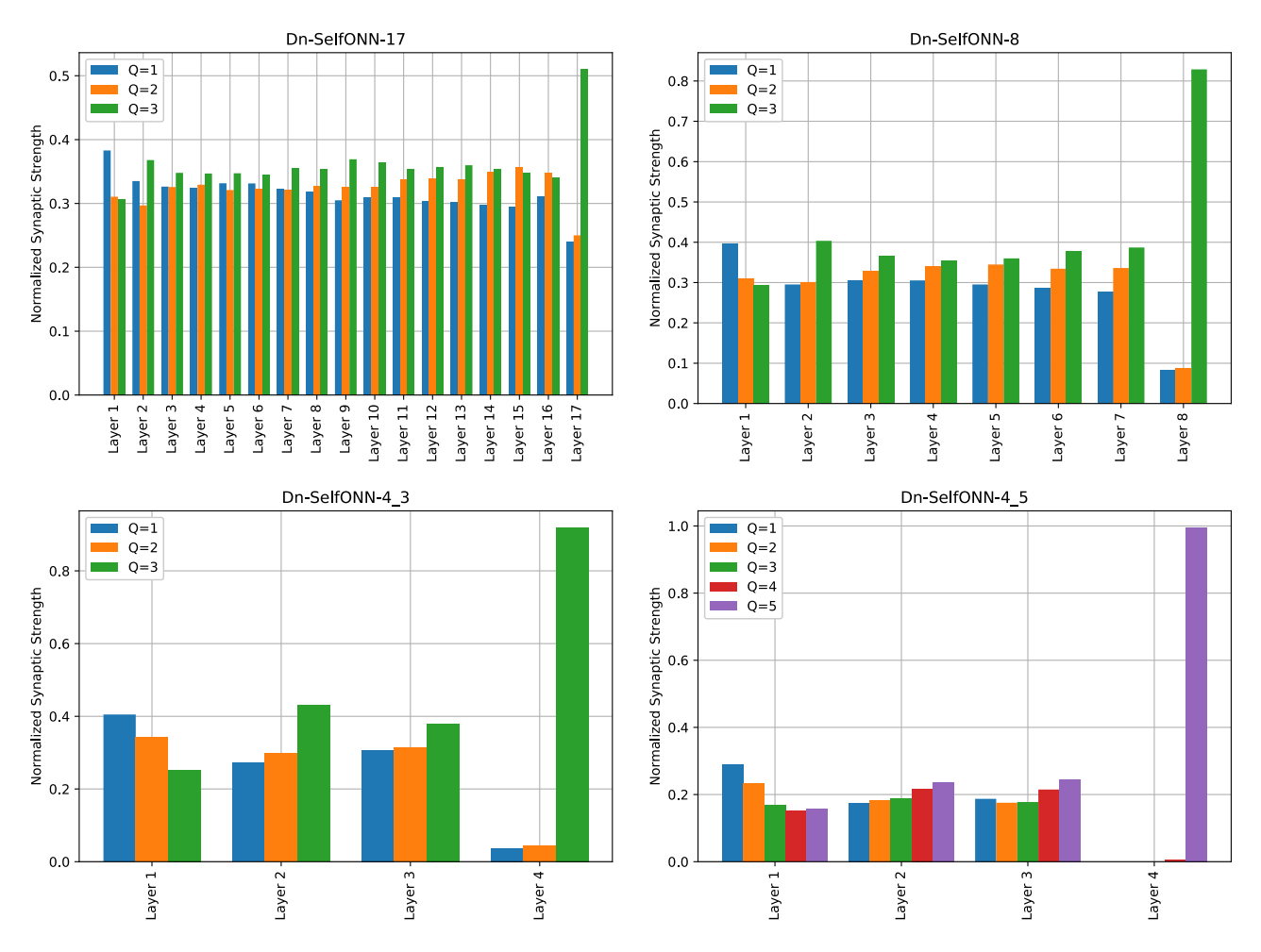


Figure 5. Distribution of weights corresponding to different Q values in the Self-ONN networks used in this study.

D. Non-linearity Analysis

1) Inter-layer differences in non-linearity

In Figure 5, we analyze the distribution of learned nonlinearities between the layers of the trained network. For representing the power of weights, we simply use the variance as a direct measure of the relative impact or synaptic strength of each order of weights. This has been found useful in earlier studies dealing with operator optimization of ONNs [15]. Recall from Section III, that O=1 corresponds to the weights of the convolutional neuron, whereas weights for Q>1 are responsible for encoding non-linearity into the transformation. Therefore, we plot the variance of subsets of weights corresponding to different Q values. From Figure 5, we immediately notice clear trends that are consistent across different network topologies. The input layer seems to always favor the linear convolution model as all three Self-ONN networks, Dn-SelfONN-17, Dn-SelfONN-8, and Dn-SelfONN-4 have the highest variance for O=1 weights for the input layer. Interestingly, the opposite is observed for the output layer. Specifically, all three networks tend to exclusively favor the higher-order weights, pointing towards a greater need for non-linearity. As outlined in earlier works [12], [16], this is one of the key benefits of Self-ONN. As compared to ONNs where the output layer operator is fixed, Self-ONNs can generate the required non-linear transformation for the output layer like any other layer in the network. Overall, the tendency of denoising Self-ONN networks to incline towards a linear (convolutional) model for the input layer and a highly non-linear transformation for the output layer provides evidence that the naïve approach of using the same Q value for all layers is sub-optimal and a better approach would be to use a lower value of Q for layers closer to the input and a higher value only for the last few layers. This will also have an additional benefit of decreasing the total number of trainable parameters, especially in the case of deep networks

2) Effect of depth on non-linearity

Earlier works [12], [16] have shown how ONNs and Self-ONNs, can learn sufficiently well with compact networks and surpass the linear model of CNNs. This ability is often attributed to the fact that Self-ONNs can incorporate higher

non-linearity even in small network architectures. As this is the first study dealing with deep Self-ONNs, it is worth analyzing how the trained deep networks make use of the available non-linear transformations and differ from the corresponding compact networks trained for the same problem. To assess this, we measure the synaptic strength of connections corresponding to different O values for Self-ONN networks, as shown in Figure 6. For the deepest network, Dn-SelfONN-17, the strengths corresponding to the three Q values are distributed approximately evenly with Q>1 weights slightly overpowering Q=1 weights. For Dn-SelfONN-8, we start noticing the need for higher nonlinearities as Q=3 connections are stronger compared to Q=2 and the convolutional (Q=1) connections. Finally, for the compact 4-layer network, the need for non-linearity is greatly increased, reflected by more than the 2-times increase in the synaptic strength from Q=2 to Q=3, and more than the 4times increase for the case of convolutional (O=1) connections. This is another evidence towards the premise that the convolutional neuron model is inherently suited for deeper networks and is not expressive enough to learn meaningful representations in the compact domain.

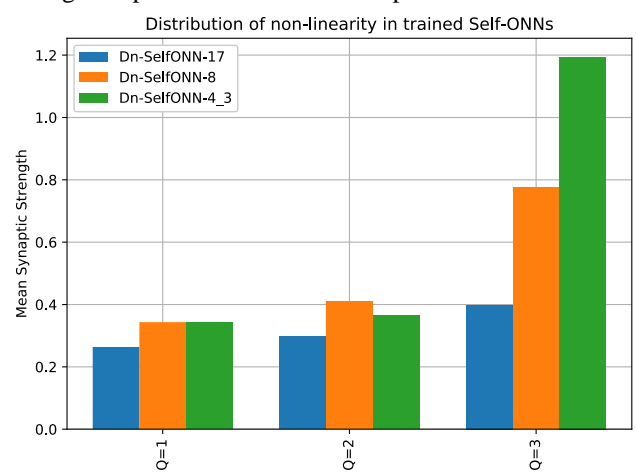


Figure 6. The extent of learned non-linearity for the Self-ONN networks with different depths.

E. Computational Complexity Comparison

In this section, we present a comparison of the computational complexity of both Self-ONNs and CNNs. To this end, we first introduce the formulation used to calculate the total number of FLOPs for both CNN and Self-ONN. Afterward, we provide a discussion regarding the parallelizability of the operations and its impact on the inference times of the networks. For the sake of brevity, we assume the 'same' convolution with unit stride and zero dilation, so the layers' input and output spatial resolution are kept identical. As none of the networks used in this study use bias, we omit that in our formulation.

Given a layer l in the network architecture, we denote the number of neurons in the current layer (output channels) as N_l and the number of neurons in the previous layer (input

channels) as N_{l-1} . For the first (input) layer, N_{l-1} corresponds to the number of channels in the input image (3 for this study). The kernel size is assumed to be $K \times K$ and the spatial resolution of the input (and output) is $H \times W$. The number of FLOPs required for the CNN layer is now given by the following formula:

$$FLOPs_{CNN}^{l} = (H * W)(K^{2}N_{l-1}N_{l} + (K^{2} - 1)N_{l-1}N_{l})$$
(28)

The terms $K^2N_{l-1}N_l$ and $(K^2-1)N_{l-1}N_l$ represent the total number of multiplication and addition operations required for the kernel operations of this layer, respectively. As each pixel in the output requires kernel operations from all the neurons, the above terms are multiplied by the number of pixels in the output. This can be visually verified from (15). Now, for an operational layer, we can use the same notation. Note from (27) that the Self-ONN formulation can be represented as a convolution operation with Q-times more input channels than the CNN layer, albeit with an additional cost of achieving the Hadamard exponentiation operation of (20). Taking this into account, we can write the total cost of a Self-ONN layer in terms of the number of FLOPs as follows:

$$FLOP s_{SelfONN}^{l} = ((H * W)(K^{2}N_{l-1}QN_{l} + (K^{2} - 1)N_{l-1}QN_{l}))$$

$$+ FLOP s_{exp}^{Q}$$
(29)

where $FLOPS_{exp}^Q$ are the multiplication operations required to achieve the Hadamard exponentiation and are calculated as follows:

$$FLOPs_{exp}^{Q} = H * W * N_{l-1} * T(Q-1)$$
 (30)

In (30), T(Q-1) denotes the $(Q-1)^{th}$ triangular number and is calculated as $\sum_{k=1}^{Q-1} k$. Note that this assumes that all higher powers of the input are calculated independently from each other and do not reuse the previous power i.e. x^q is calculated as $\prod_{1}^{q} x$ instead of $x^{q-1}x$. Despite being apparently redundant, this is important to preserve the independence of the operations because reusing previous powers entails waiting for all q-1 powers before finally calculating x^q . In practice, this will enable efficient exploitation of parallel computing resources such as CUDA cores.

Finally, using (30), the number of FLOPS required for a Self-ONN layer can be calculated. Table 4 provides the number of FLOPS for all networks used in this study. Note that the computational cost of activation functions and BatchNorm layers are omitted as they have the same parameters for both CNN and Self-ONN layers and roughly add a constant number of FLOPS. It is key to note here that the total number of FLOPS, despite wide-scale usage, lacks a definitive factor that ultimately determines the efficiency of the network - the parallelizability factor. Specifically, the ratio of operations in the network which are independent of each other, and hence can be parallelized in an ideal setting,

is not accounted for. Therefore, in practice, FLOPS alone cannot be used as a sole measure of network efficiency.

Table 4. Number of FLOPs and the running times for the
denoising networks used in this study.

	FLOPs	Running Time (ms)		
	(G)	256x256	512x512	
DnCNN	68.88	11.720	41.888	
Dn-SelfONN-17	207.04	24.757	92.925	
Dn-SelfONN-8	83.60	10.691	39.539	
Dn-SelfONN-4_3	28.74	4.433	15.789	
Dn-SelfONN-4 5	47.96	6.366	23.389	

For example, given the availability of enough parallel computing resources, a model requiring F number of FLOPs (distributed evenly among the layers), composed of 10 layers can only achieve F/10 FLOPS in a unit time because each intermediate layer is dependent on the output of the previous layer. However, for a 2-layer network with the same number of FLOPs, F/2 FLOPS can be calculated in a unit time, resulting in a 5-fold theoretical speed-up as compared to the 10-layer network. Therefore, the shallower denoising networks used in this study, Dn-SelfONN-8 and Dn-SelfONN-4 lend themselves to more efficient parallelization. Even though the current Self-ONN implementation is not optimized to fully exploit the independence of operations, we can see the above effect reflected quite clearly in the empirical observations of the running times of the different networks in Table 4. For example, we see that Dn-SelfONN-4 5, despite having 67% more FLOPs compared to Dn-SelfONN-4 3, results in an increase of only 43% in terms of running time. More importantly, Dn-SelfONN-8 with 8layers, despite requiring 21% more FLOPs compared to the 17-layer CNN, achieves more than 8% decrease in running time. In general, the running times of the GPU-powered SelfONNs can be further reduced if a fused kernel approach is adopted, such that the Hadamard exponentiation operation and the convolution are carried out by the same CUDA kernel.

VI. CONCLUSION

This study proposes novel Self-ONNs by using operational layers as an effective drop-in replacement for convolutional layers. In this way, even in deep architectures, the resulting Self-ONNs are demonstrated for the first time to achieve a superior denoising performance than the current state-of-theart deep CNN model, DnCNN. Moreover, a similar or even better performance level of DnCNN can still be achieved by Self-ONNs using a fraction of the layers and neurons. This questions the need for creating very deep and complex networks since this study has clearly shown that the required diversity and learning/generalization capability can also be accomplished by the proposed self-organized "heterogeneous" networks with compact configurations both in terms of network depth and the total number of learning units (neurons). Furthermore, this study has revealed that in deep as well as relatively compact networks, the need for

non-linearity is higher for layers closer to the output layer compared to layers closer to the input layer. The study also revealed that for the denoising problem, compact Self-ONNs require more non-linearity (higher Q) to stay competitive with deeper networks. Optimizing the amount of nonlinearity per-layer in an unsupervised manner remains a key challenge towards further improving the performance of Self-ONNs and reducing their network complexity. The additional FLOPs required for achieving the Self-ONN formulation include mostly independent operations which lend themselves to more efficient parallelization compared to CNNs. Unsupervised adaptation of layer-wise non-linearity and a more efficient implementation remain open topics to be tackled in future extensions of this work. Finally, we also find evidence that training data has a profound impact on the performance of discriminative learning-based methods. Therefore, a standardized approach towards a fair benchmarking of new architectures is recommended.

VII. REFERENCES

- [1] J. Portilla, V. Strela, M. J. Wainwright, and E. P. Simoncelli, "Image denoising using scale mixtures of Gaussians in the wavelet domain," *IEEE Trans. Image Process.*, 2003.
- [2] I. Tăbuş, D. Petrescu, and M. Gabbouj, "A training framework for stack and Boolean filtering Fast optimal design procedures and robustness case study," *IEEE Trans. Image Process.*, 1996.
- [3] H. C. Burger, C. J. Schuler, and S. Harmeling, "Image denoising: Can plain neural networks compete with BM3D?," in *Proceedings of the IEEE Computer Society Conference on Computer Vision and Pattern Recognition*, 2012.
- [4] K. Zhang, W. Zuo, Y. Chen, D. Meng, and L. Zhang, "Beyond a Gaussian denoiser: Residual learning of deep CNN for image denoising," *IEEE Trans. Image Process.*, 2017.
- [5] T. Plötz and S. Roth, "Benchmarking denoising algorithms with real photographs," in *Proceedings 30th IEEE Conference on Computer Vision and Pattern Recognition, CVPR 2017*, 2017.
- [6] A. Foi, M. Trimeche, V. Katkovnik, and K. Egiazarian, "Practical Poissonian-Gaussian noise modeling and fitting for single-image raw-data," *IEEE Trans. Image Process.*, 2008.
- [7] F. Luisier, T. Blu, and M. Unser, "Image denoising in mixed poissongaussian noise," *IEEE Trans. Image Process.*, 2011.
- [8] Y. Zhou *et al.*, "When AWGN-based Denoiser Meets Real Noises," Apr. 2019.
- [9] A. Abdelhamed, S. Lin, and M. S. Brown, "A High-Quality Denoising Dataset for Smartphone Cameras," in *Proceedings of the IEEE Computer* Society Conference on Computer Vision and Pattern Recognition, 2018.

- [10] J. Anaya and A. Barbu, "RENOIR A dataset for real low-light image noise reduction," *J. Vis. Commun. Image Represent.*, 2018.
- [11] S. Kiranyaz, T. Ince, A. Iosifidis, and M. Gabbouj, "Operational neural networks," *Neural Comput. Appl.*, 2020.
- [12] J. Malik, S. Kiranyaz, and M. Gabbouj, "Self-organized operational neural networks for severe image restoration problems," *Neural Networks*, 2020.
- [13] C. Wang, J. Yang, L. Xie, and J. Yuan, "Kervolutional Neural Networks."
- [14] G. Zoumpourlis, A. Doumanoglou, N. Vretos, and P. Daras, "Non-linear Convolution Filters for CNN-Based Learning," in *Proceedings of the IEEE International Conference on Computer Vision*, 2017.
- [15] S. Kiranyaz, J. Malik, H. B. Abdallah, T. Ince, A. Iosifidis, and M. Gabbouj, "Exploiting Heterogeneity in Operational Neural Networks by Synaptic Plasticity," *Neural Comput. Appl.*, vol. November, 2020.
- [16] S. Kiranyaz, J. Malik, H. Ben Abdallah, T. Ince, A. Iosifidis, and M. Gabbouj, "Self-Organized Operational Neural Networks with Generative Neurons." 2020.
- [17] S. Nam, Y. Hwang, Y. Matsushita, and S. J. Kim, "A Holistic Approach to Cross-Channel Image Noise Modeling and Its Application to Image Denoising," in *Proceedings of the IEEE Computer Society Conference on Computer Vision and Pattern Recognition*, 2016.
- [18] K. Dabov, A. Foi, V. Katkovnik, and K. Egiazarian, "Image restoration by sparse 3D transform-domain collaborative filtering," in *Image Processing:* Algorithms and Systems VI, 2008.
- [19] S. W. Zamir et al., "Learning Enriched Features for Real Image Restoration and Enhancement," in Lecture Notes in Computer Science (including subseries Lecture Notes in Artificial Intelligence and Lecture Notes in Bioinformatics), 2020.
- [20] S. Anwar and N. Barnes, "Real image denoising with feature attention," in *Proceedings of the IEEE International Conference on Computer Vision*, 2019.
- [21] S. Guo, Z. Yan, K. Zhang, W. Zuo, and L. Zhang, "Toward convolutional blind denoising of real photographs," in *Proceedings of the IEEE Computer Society Conference on Computer Vision and Pattern Recognition*, 2019.
- [22] C. Chen, Z. Xiong, X. Tian, Z. J. Zha, and F. Wu, "Real-World Image Denoising with Deep Boosting," *IEEE Trans. Pattern Anal. Mach. Intell.*, 2020.
- [23] D. W. Kim, J. R. Chung, and S. W. Jung, "GRDN:Grouped residual dense network for real image denoising and GAN-based real-world noise modeling," in *IEEE Computer Society Conference on Computer Vision and Pattern Recognition Workshops*, 2019.

- [24] S. W. Zamir et al., "CycleISP: Real image restoration via improved data synthesis," in *Proceedings of the IEEE Computer Society Conference on Computer Vision and Pattern Recognition*, 2020.
- [25] Y. Song, Y. Zhu, and X. Du, "Grouped Multi-Scale Network for Real-World Image Denoising," *IEEE Signal Process. Lett.*, 2020.
- [26] J. Malik, S. Kiranyaz, and M. Gabbouj, "FastONN Python based open-source GPU implementation for Operational Neural Networks," *arXiv*. 2020.
- [27] Y. Chen and T. Pock, "Trainable Nonlinear Reaction Diffusion: A Flexible Framework for Fast and Effective Image Restoration," *IEEE Trans. Pattern Anal. Mach. Intell.*, 2017.
- [28] K. Zhang, W. Zuo, and L. Zhang, "FFDNet: Toward a fast and flexible solution for CNN-Based image denoising," *IEEE Trans. Image Process.*, 2018.
- [29] J. Xu, L. Zhang, and D. Zhang, "A trilateral weighted sparse coding scheme for real-world image denoising," in Lecture Notes in Computer Science (including subseries Lecture Notes in Artificial Intelligence and Lecture Notes in Bioinformatics), 2018.